JOURNAL OF PROPULSION AND POWER
Vol. 9, No. 4, July–Aug. 1993

Scramjet Nozzle Experiment with Hypersonic External Flow

Shigeya Watanabe*
National Aerospace Laboratory, Chofu, Tokyo 182, Japan

An experimental study of scramjet asymmetric nozzle flowfields is conducted to investigate the effects on nozzle performance of interactions between engine exhaust and hypersonic external flow. The test model consists of a flat-plate ramp and a short cowl. Tests are performed in a hypersonic wind tunnel (M_∞ = 7.1) whose freestream constitutes the external flow around an aerospace plane. Room temperature air is used to simulate engine exhaust flow. Model surface pressure and pitot pressure distributions in the flowfields are measured, from which nozzle performance is calculated. Flow visualizations are performed using several techniques. It is found that in underexpansion conditions, the external flow affects the model surface pressure only from the ramp sides because the intercepting shock (barrel shock) does not impinge upon the ramp surface. It is shown that the external flow produces an effect which suppresses boundary-layer separation on the ramp surface. When using a long side fence (SF), spanwise expansion of the exhaust flow is restrained, thus, a slight gain of thrust can be obtained relative to that using a shorter side fence. The predicted nozzle performance by the two-dimensional method of characteristics with boundary-layer correction agrees well with the long side fence experimental results.

Nomenclature

L = lift acting on nozzle
M = Mach number or pitching moment acting on nozzle around c.g.
p = static pressure
T = thrust acting on nozzle
x = distance from model throat in freestream direction
y = spanwise distance from model centerline

Subscripts
ce = combustor exit
ine = internal nozzle exit
MOC = method of characteristics
pc = plenum chamber
sp = separation point
t = stagnation condition
∞ = freestream or ambient condition

Introduction

ENGINE-AIRFRAME integration is a key technology to develop a single-stage-to-orbit (SSTO) aerospace plane with scramjet propulsion. The forebody of an integrated SSTO vehicle acts as an inlet compression surface, whereas the afterbody comprises an external nozzle surface.

The external nozzle surface has an asymmetric configuration due to having only an upper solid surface; hence, the lower region of the scramjet engine exhaust flow interacts with the hypersonic airflow around the vehicle. Since the net thrust in the operational speed range of the scramjet engine is rather small relative to the overall thrust, the nozzle thrust must be accurately predicted, including the effect of the interaction of the exhaust and the external flow.

Simulating the complex, chemically reacting flows around the external nozzle is extremely difficult using ground test facilities, and so investigations on scramjet nozzles have been primarily conducted by computational fluid dynamics techniques.[1–4] In fact, experimental studies of the scramjet nozzle flow[5–8] are limited, and the majority of them deal with only the engine exhaust flow.[5,6]

This led to the present study which experimentally investigates both the engine exhaust and the external flowfields of an asymmetric scramjet nozzle model. The first objective of this study is to investigate the complex structure of the flowfield where the exhaust and the external flows interact in order to establish a nozzle performance prediction method for parametric design studies which includes the interaction effects. The second is to study the effects of several design parameters on nozzle performance, e.g., side fence (SF) length and pressure ratio of the exhaust to the external flow. For these purposes the surface pressure on a scramjet nozzle model and the pitot pressure distribution in the flowfield were precisely measured. All the experiments were performed in a low-enthalpy hypersonic wind tunnel using cold air to simulate the exhaust flow, therefore, only perfect gas conditions are considered with the effects of chemical reactions and specific heat ratio variations in the exhaust flow being neglected.

Apparatus and Tests

Scramjet Nozzle Model

Figure 1 shows a schematic of the scramjet asymmetric nozzle model which is inverted in comparison with that in an actual vehicle. The model is comprised of an internal nozzle, which is a duct between the combustor exit station and the cowl trailing edge, and an external nozzle consisting of a flat ramp surface located behind the internal nozzle. The model configuration was designed using a conceptual SSTO design study.[9] The inclination angles of the ramp and the cowl inner and outer surfaces are 20, 10, and 5 deg, respectively. Design Mach number values at the combustor and internal nozzle exits are 2.5 and 3, respectively. Side extension plates attached to the ramp width were used to simulate the external flow in the engine-side regions. Three side fences of different lengths were interchangeably used. The short side fence, SF-1, was used for visualization of the internal nozzle flow, whereas SF-2 and SF-3 were used to investigate the effects of side fence length on nozzle performance. In most tests, the medium-length side fence SF-2, whose trailing edge coincides with the cowl trailing edge, was used with the side extension plates. Simulated exhaust flow is supplied through a lower

Presented as Paper 92-3289 at the AIAA/SAE/ASME/ASEE 28th Joint Propulsion Conference, Nashville, TN, July 6–8, 1992; received Aug. 13, 1992; revision received March 16, 1993; accepted for publication March 17, 1993.

*Researcher, Aerodynamics Division, 7-44-1 Jindaiji-higashi-machi. AIAA Member.

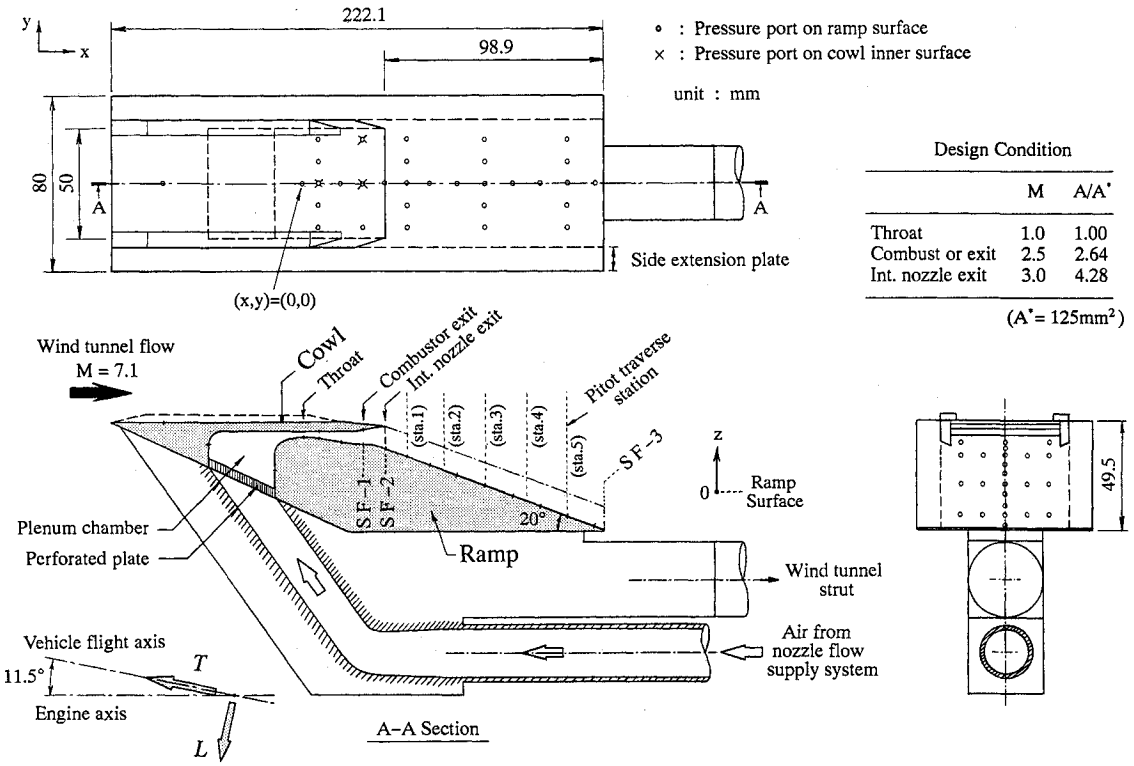

Fig. 1 Scramjet asymmetric nozzle model.

Table 1 Test conditions

Case	M_{flight}	p_{cc}/p_∞	p_{inc}/p_∞	M_∞	α, deg	p_{pc}, kPa	$p_{r\infty}$, kPa	Condition at internal nozzle exit
1	10	13.1	6	7.1	0	145	2940	Underexpansion
2	——	3.5	1.6	7.1	0	39	2940	Underexpansion
3	——	0.9	0.4	7.1	0	10	2940	Overexpansion
4	8.5	12.6	5.8	6.4	4	140	1470	Underexpansion

pipe, stagnates in a plenum chamber, and is accelerated through the throat to supersonic speeds.

Flow Simulation Apparatus

Experiments were conducted in the National Aerospace Laboratory (NAL) 50-cm-diam blowdown-type hypersonic wind tunnel at a freestream Mach number of 7.1 and a Reynolds number of 1.02×10^6, which is referenced by the external nozzle length. The stagnation temperature was regulated at about 400°C, and the wind-tunnel duration was 120 s in the present tests. Detailed information of this facility is reported in Ref. 10. The freestream air of the wind tunnel simulated the hypersonic external flow, whereas room temperature dry air from the nozzle flow supply system simulated the engine exhaust flow. Since air was used as the exhaust due to the limitation of the experimental instruments, the exhaust's specific heat ratio γ is different from that of the high-temperature combustion gas in an actual scramjet engine; hence in this regard, the experimental flowfields do not meet similar flow conditions[7] with actual flight flowfields.

At a wind-tunnel freestream Mach number of 7.1 and an exhaust-to-external flow pressure ratio at the internal nozzle exit (p_{inc}/p_∞) of 6, actual flight conditions can be simulated for Mach 10 at an altitude of 28.6 km with an angle of attack of 3.4 deg.

Measurements

Ramp and cowl surface pressure were measured at 35 points. Pitot pressure distributions in the interacting flowfields were measured at five stations (Fig. 1) using a traverse system and a rake consisting of 11 horizontal pitot pressure tubes at intervals of 1 cm. These surface pressure distribution measurements enabled nozzle performance parameters to be calculated, e.g., thrust, drag, and pitching moment.

Table 1 shows the test conditions, where case 1 is the basic case simulating a Mach 10 flight condition. Cases 2 and 3 have different pressure ratios p_{inc}/p_∞ to study the effects of this ratio on the flowfields. Case 4 has a slightly lower simulated Mach number ($M_{flight} = 8.5$) than that in case 1, and this test condition was obtained by inclining the model by 4 deg to decelerate the external flow. Additional tests in which the nozzle exhaust was injected into quiet ambient air, i.e., without the external flow, were also conducted to more clearly investigate the external flow effects.

Four types of three-dimensional flow visualization techniques were used: 1) schlieren, 2) shadowgraph, 3) surface oil flow, and 4) vapor screen techniques. The shadowgraph test utilized a xenon discharge tube with 1.6-μs duration. Small, constant-volume oil dots were used in the surface oil flow test to indicate both flow directions and the magnitude of shear stress on the model surface. Vapor screen tests were conducted by slightly condensing the wind-tunnel freestream under a low stagnation temperature condition. Through these vapor screen tests, it was confirmed that the airflow simulating the engine exhaust did not condense.

Results and Discussion

Results for Basic Case (Case 1)

The results for case 1, using SF-2, are presented in this section. The surface pressure distribution at the model cen-

terline is shown in Fig. 2, with pressure being nondimensionalized by the plenum chamber pressure p_{pc}. The pressure on the ramp monotonously decreases in the exhaust flow direction, except near the ramp aft end where it increases due to a shock induced by boundary-layer separation. On the other hand, the cowl surface has an adverse pressure gradient near the trailing edge, which is caused by compression waves generated on the excessively concave ramp surface near $x = 2$ cm.

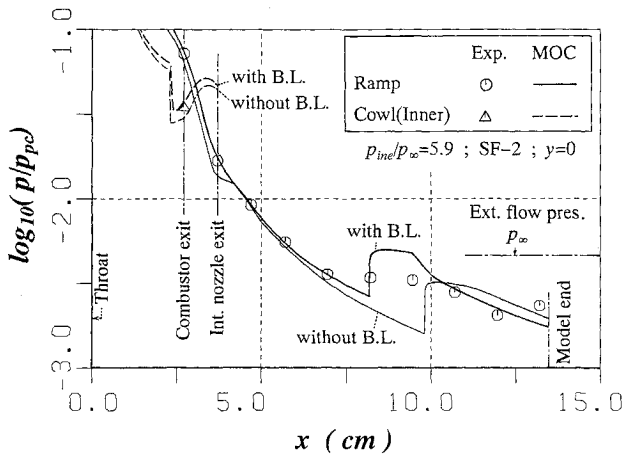

Fig. 2 *Surface pressure at model centerline for case 1.*

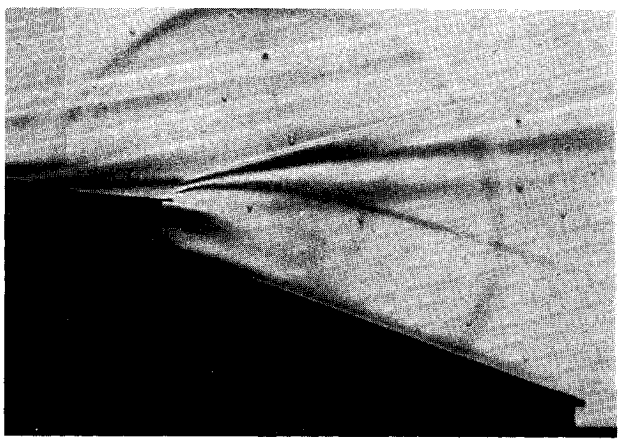

Fig. 3 Schlieren photograph for case 1 (p_{ine}/p_∞ = 5.9; SF-2).

Figure 2 also shows the two-dimensional method of characteristics (MOC) results with and without a boundary-layer displacement thickness correction. The boundary layers on the ramp and cowl were assumed to be turbulent, the displacement thickness was calculated by the method of Ref. 11, and the effects of the external flow are not included. The calculated pressure with the boundary-layer correction agrees well with the experimental results on the ramp forward surface and cowl inner surface. In contrast, on the rear portion of the ramp surface, correlation is poor because of boundary-layer separation and the impingement of a weak shock generated on the cowl inner surface.

Figure 3 shows a schlieren photograph which clearly shows a two-dimensional flowfield on the symmetrical plane. An external plume shock from the cowl trailing edge, a shear layer between the exhaust and the external flow, and an intercepting shock (barrel shock) in the exhaust flow can be seen. The intercepting shock is similar to that observed in supersonic underexpanded free jets into still air.[12] Because the boundary layer on the cowl upper surface abruptly thickens near the cowl trailing edge, a boundary-layer separation is inferred. Figure 4 illustrates this two-dimensional flowfield.

A shadowgraph photograph is shown in Fig. 5 and clearly indicates that the shear layer is turbulent and its origin is at the thick boundary layer on the cowl upper surface. Figure 6 shows a variation in shear layer thickness determined from the schlieren photograph and pitot pressure measurements. The shear layer almost linearly thickens in the downstream direction. This linear spreading characteristic is similar to the compressible turbulent shear layer between two supersonic flows at different speeds,[13,14] whereas the spreading rate in this experiment is much higher than that estimated by the semiempirical method using a convective Mach number.[13]

Figure 7 shows surface pressure contours on the ramp. The leading expansion waves from the side fence trailing edges are also indicated, being calculated using the Mach number of the exhaust flow close to the ramp surface. Though the exhaust flow is two-dimensional forward of the internal nozzle exit, it becomes three-dimensional in downstream flow due to the expansion waves and intercepting shocks from the side fence trailing edges. A pressure decrease in the ramp side regions begins in front of the estimated leading expansion waves because of the existence of the boundary layer having a lower Mach number. An oil flow photograph on the ramp and cowl upper surface is shown in Fig. 8. Crossflow separation of the exhaust flow is apparent in the ramp side regions. It is believed that this separation is induced by the interaction

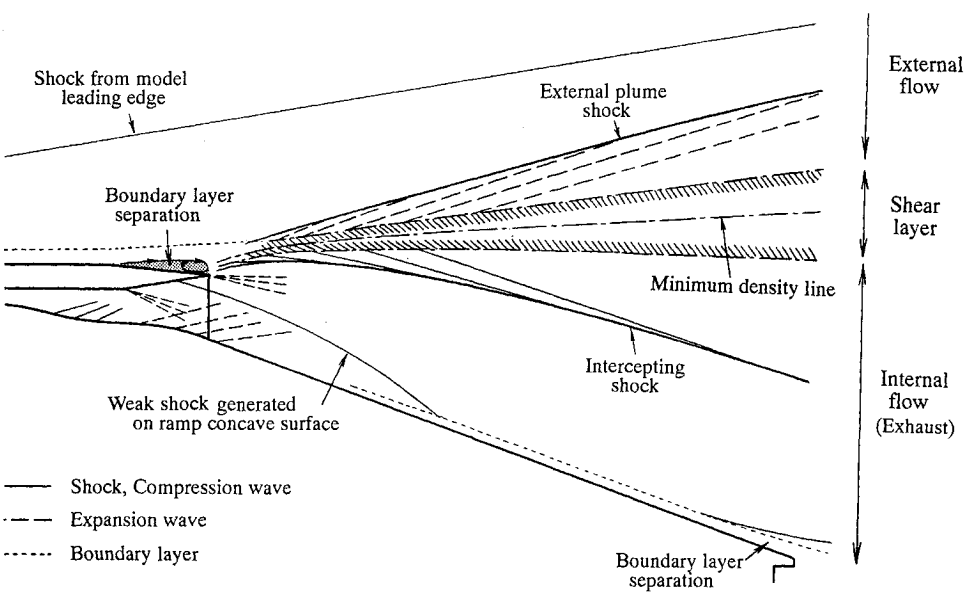

Fig. 4 Two-dimensional flowfield on model symmetrical plane (y = 0) for case 1 (p_{ine}/p_∞ = 5.9; SF-2).

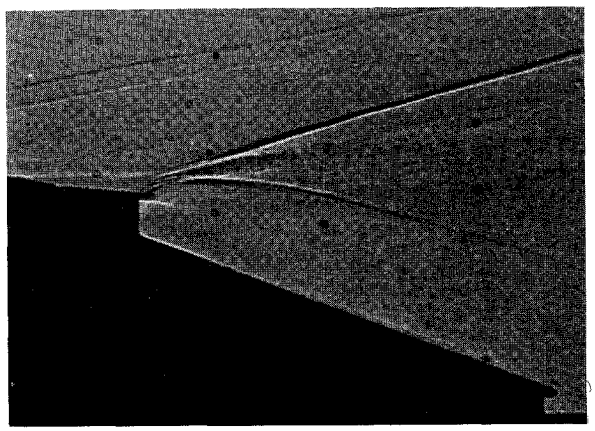

Fig. 5 Shadowgraph photograph for case 1 (p_{ine}/p_∞ = 5.9; SF-2).

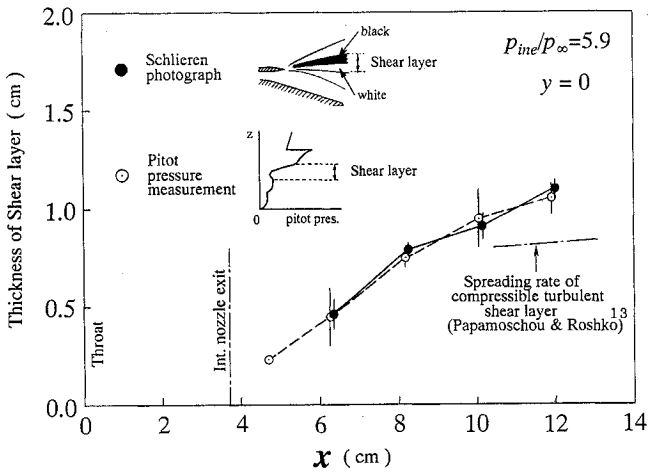

Fig. 6 Thickness variation of shear layer for case 1.

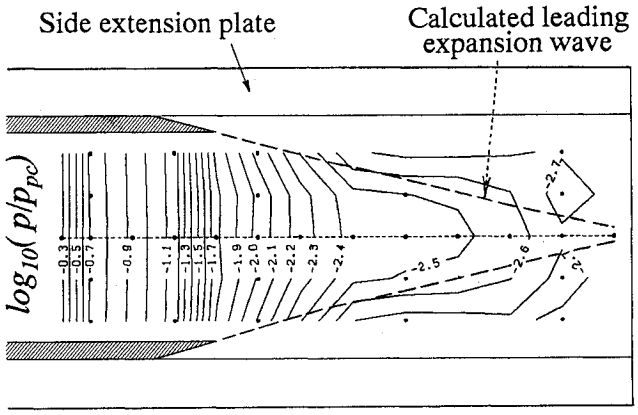

Fig. 7 Ramp surface pressure contours for case 1 (p_{ine}/p_∞ = 5.9; SF-2).

of the boundary layer with the intercepting shock from the trailing edge of the side fence. The separated crossflow forms a vortex which reattaches near the ramp side edge and causes secondary separation. A low-shear region exists between the crossflow separation line and the secondary separation line, as well as near the ramp aft end. The external flow forms a vortex at the ramp side edge which reattaches on the ramp surface near the side edge. On the cowl upper surface near the trailing edge, primary and secondary separation lines occur having a low shear region between them. Figure 9 is a cross-sectional schematic showing the flowfield as inferred from the oil flow and vapor screen results. Several vortices are produced at the expansion corners of the side extension plates and at upper corners of the internal nozzle exit. Further

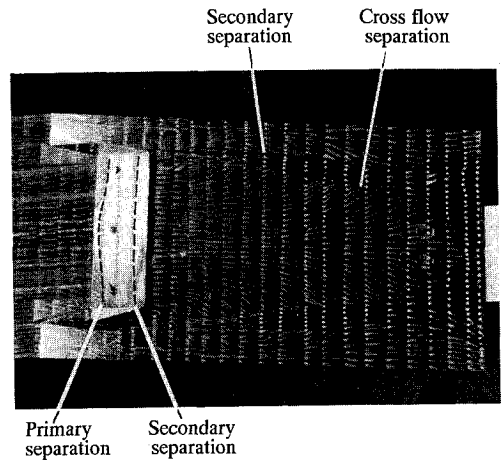

Fig. 8 Oil flow photograph for case 1 (p_{ine}/p_∞ = 5.9; SF-2).

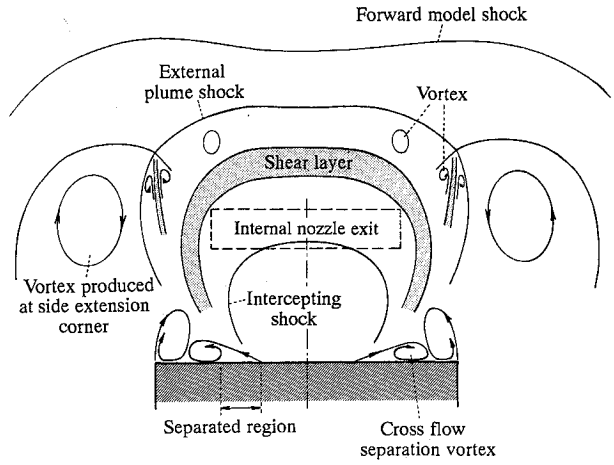

Fig. 9 Cross-sectional schematic of nozzle flowfield for case 1 (x = 12 cm; p_{ine}/p_∞ = 5.9; SF-2).

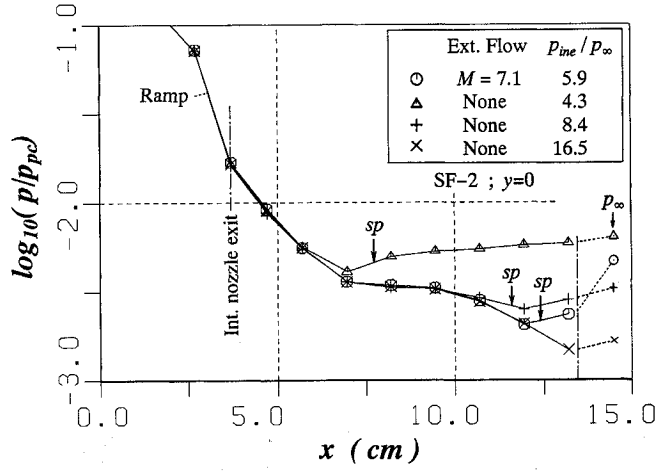

Fig. 10 Comparison of centerline surface pressure with and without external flow.

flowfield measurements and visualizations are necessary to fully explain the detailed flowfield structure.

External Flow Effects on Flowfield

A comparison of the centerline surface pressure distributions with and without external flow is shown in Fig. 10. The tests without external flow were carried out under several different pressure ratios p_{ine}/p_∞. The surface pressure distribution with external flow is identical to that without external flow at p_{ine}/p_∞ = 16.5, except near the ramp aft end region

which is affected by the separation shock. This indicates that the information of the external flow from the cowl trailing edge does not reach the ramp on the centerline. It should be noted that with external flow the surface pressure near the ramp aft end is much lower than the freestream static pressure, whereas without external flow it is almost equal to ambient pressure. This fact indicates the external flow has an effect to delay the boundary-layer separation near the ramp aft end by reducing the pressure on the ramp base region. Figure 11 shows a schlieren photograph without external flow at $p_{ine}/p_\infty = 4.3$. The flowfield structure is qualitatively similar to that with external flow, except for the absence of the external plume shock. By comparison with Fig. 3, it is obvious that the upward expansion of the exhaust plume is suppressed by the pressure increase of the external flow through the external plume shock. With external flow, the upward expansion angle of the exhaust at the cowl trailing edge is smaller by 5–10 deg than that without external flow for the same pressure ratio p_{ine}/p_∞.

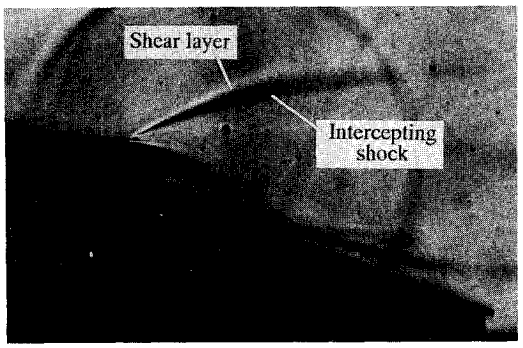

Fig. 11 Schlieren photograph without external flow (p_{ine}/p_∞ = 4.3; SF-2).

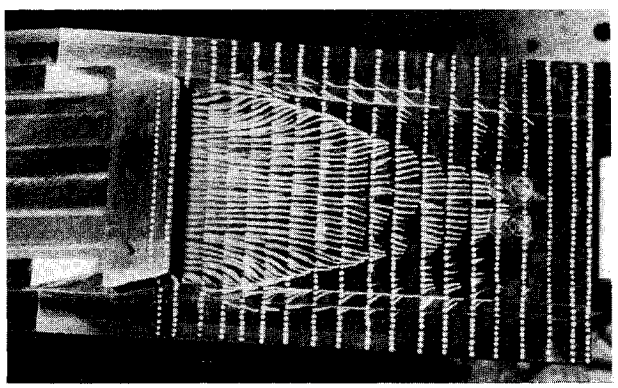

Fig. 12 Oil flow photograph without external flow (p_{ine}/p_∞ = 5.9; SF-2).

Figure 12 shows an oil flow photograph without external flow when the pressure ratio p_{ine}/p_∞ is the same as case 1 with external flow (Fig. 8). A crossflow separation of the exhaust flow is observed, as well as with the external flow, though the separation line is comparatively closer to the center and more forward than with external flow. This position difference in the separation line means the surface pressure on the ramp side and aft regions is also different, i.e., different nozzle performance is obtained.

Figure 13 compares the pitot pressure distributions on the model symmetrical plane with and without external flow. Pressure distribution below the intercepting shock is substantially the same in both cases. This evidence reinforces the conclusion that the ramp surface pressure distributions on the model centerline are identical, regardless of the existence of the external flow. The measured pressure distribution with external flow shows that expansion waves occur between the external plume shock and the shear layer, whereas weak compression waves occur between the shear layer and the intercepting shock. A hollow exists in the center of the shear layer, being caused by the momentum deficit in the thick boundary layer on the cowl upper surface, and becoming smaller in the downstream direction due to shear stress in the shear layer. The pitot pressure measurements agree well with the corresponding schlieren photograph shown in Fig. 3.

Effects of Exhaust-to-External Flow Pressure Ratio

Figure 14 compares the centerline surface pressure distributions using different pressure ratios p_{ine}/p_∞. In cases 1 and

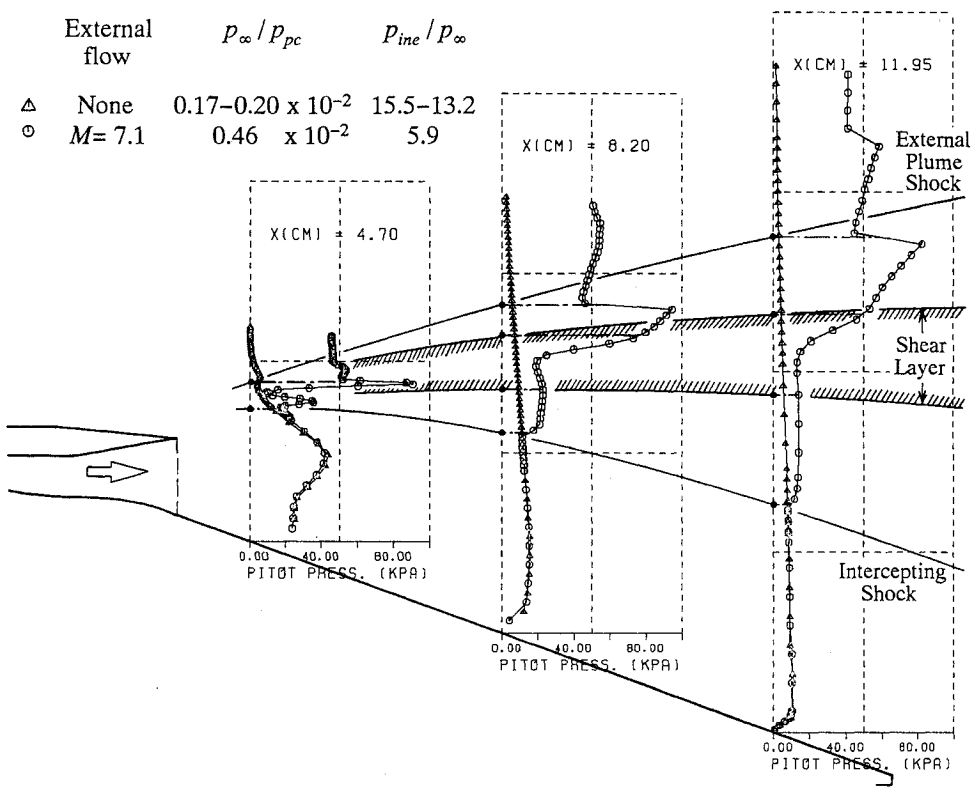

Fig. 13 Pitot pressure distributions on model symmetrical plane (y = 0).

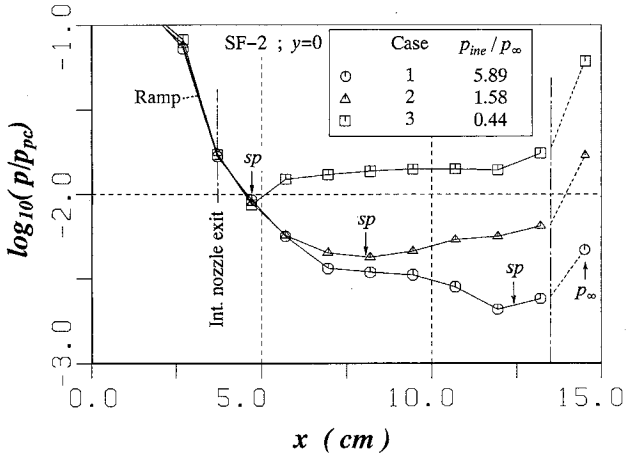

Fig. 14 Effect of pressure ratio p_{ine}/p_∞ on surface pressure at model centerline.

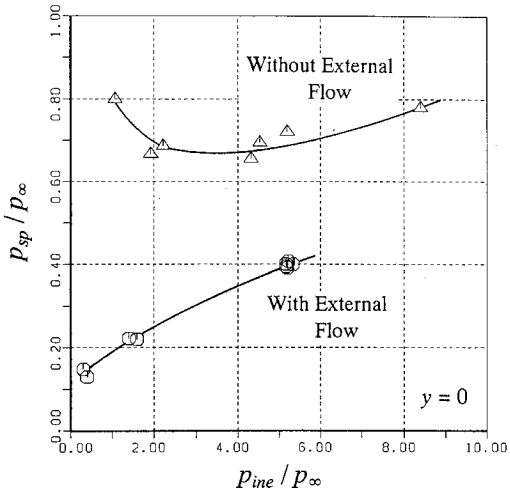

Fig. 15 Relation of pressure ratio at separation point p_{pc}/p_∞ with pressure ratio p_{ine}/p_∞.

2, the exhaust flow is in underexpansion condition at the internal nozzle exit, while it is in overexpansion condition in case 3. As the pressure ratio decreases, the point where the surface pressure on the ramp ceases to decrease, i.e., the separation point moves forward. In case 3, the ramp surface pressure abruptly increases at $x = 5$ cm, due to a sudden boundary-layer separation which is induced by impingement of a shock from the cowl trailing edge, thereby revealing that in overexpansion conditions the external flow can directly affect the ramp surface pressure on the model centerline through impingement of the shock upon the ramp. In contrast, the surface pressure in cases 1 and 2 gradually increases with the boundary-layer separation. The minimum surface pressure near the separation point is much lower than the freestream static pressure in all cases. Figure 15 shows the relationship between the separation point pressure ratio p_{sp}/p_∞ and the exhaust-to-external flow pressure ratio p_{ine}/p_∞. The value of p_{sp}/p_∞ with external flow is fairly small relative to unity, and increases with increases in p_{ine}/p_∞. On the other hand, without external flow, p_{sp}/p_∞ is close to unity and relatively constant with variations in p_{ine}/p_∞. Figure 16 shows schlieren photographs for cases 2 and 3. The upward expansion of the exhaust flow in case 2 is less than case 1 (Fig. 3), yet the intercepting shock does not impinge on the ramp as much. In case 3, the shock from the cowl trailing edge is apparent, being generated to compress the exhaust flow up to the external flow pressure. A large-scale, shock-induced separation on the ramp can also be seen in case 3. Of interest is that a weak external plume shock is present in spite of an overexpansion condition. In addition, the separation region on the cowl upper surface near the trailing edge becomes smaller with a decrease in the pressure ratio. This trend was confirmed by the oil flow tests.

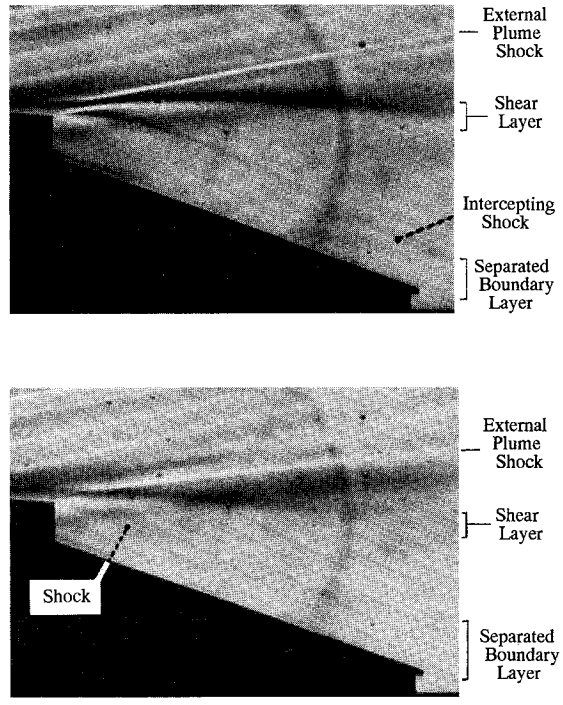

Fig. 16 Schlieren photographs with different pressure ratios p_{ine}/p_∞: a) case 2 ($p_{ine}/p_\infty = 1.58$), b) case 3 ($p_{ine}/p_\infty = 0.44$).

Effects of External Flow Mach Number

To investigate the effect of the external flow Mach number, a test using a lower external flow Mach number at the same pressure ratio as in case 1 was conducted (case 4). Schlieren photographs showed that a decrease in the Mach number caused a slight increase in the angle of the external plume shock (data not shown), with no effects on the surface pressure on the model centerline being found. The effects of the external flow Mach number on the ramp side region pressure cannot be discussed here because Mach number is not constant around the model, with the model being inclined in case 4.

Effects of Side Fence Length

Figure 17 shows the ramp surface pressure contours for SF-3, the longest length. The pressure distribution is almost two-dimensional with a slight pressure decrease in the ramp side regions, and the spanwise pressure variation is much less than with SF-2 (Fig. 7), therefore, nozzle thrust is greater. Figure 18 shows an oil flow photograph with SF-3. The streamlines between the side fences do not drift outward as with SF-2 (Fig. 8), but instead have a wave-like shape. This streamline shape indicates existence of weak shocks and expansion waves perpendicular to the ramp surface. Crossflow separation observed using SF-2 was not detected with SF-3.

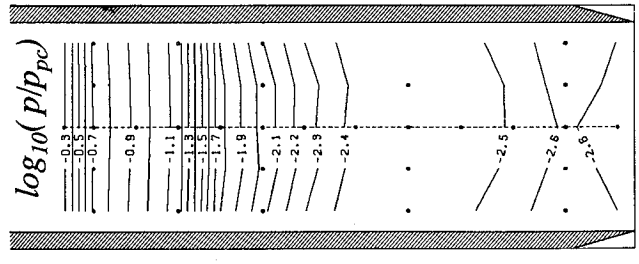

Fig. 17 Ramp surface pressure contours with SF-3 ($p_{ine}/p_\infty = 5.9$).

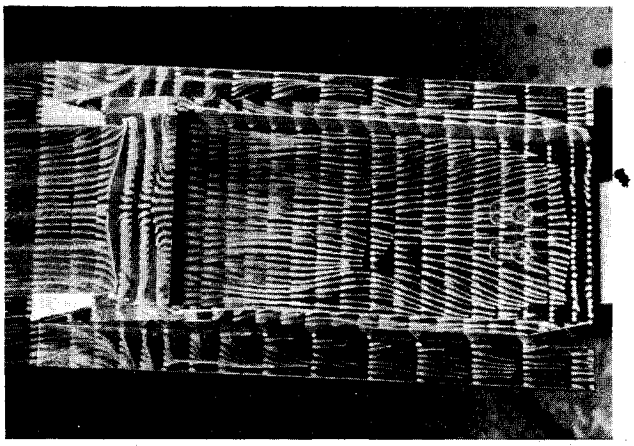

Fig. 18 Oil flow photograph with SF-3 (p_{ine}/p_∞ = 5.9).

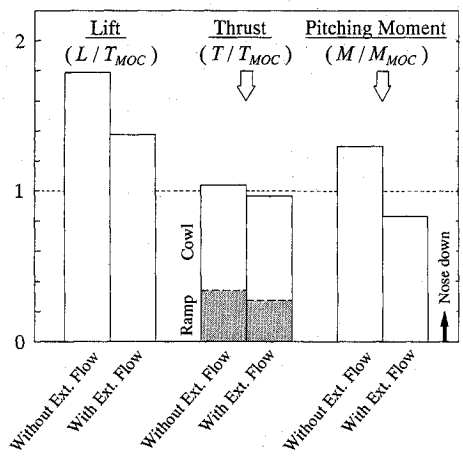

Fig. 19 Effect of external flow on nozzle performance (engine inclination angle = 11.5 deg; p_{ine}/p_∞ = 5.9; SF-2).

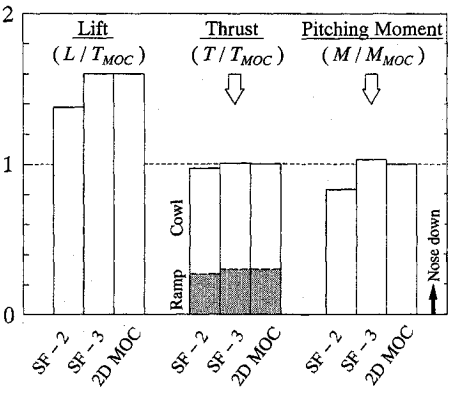

Fig. 20 Effect of side fence length on nozzle performance (engine inclination angle = 11.5 deg; p_{ine}/p_∞ = 5.9).

Nozzle Performance

Thrust, lift, and pitching moment acting on the internal and external nozzle were calculated by integrating the surface pressure measurements. Skin friction was not included here. Thrust and lift forces are nondimensionalized using an estimated value obtained by the two-dimensional method of characteristics (MOC) with a boundary-layer correction, and are defined relative to the vehicle flight direction which is 11.5-deg lower than the engine axis (Fig. 1). The pitching moment is the moment around the vehicle c.g. located at $x = -24.5$ mm, being nondimensionalized, as were the forces.

Figure 19 shows the nozzle performance with and without external flow. In both cases, the net lift, the difference between the positive lift acting on the ramp and the negative lift acting on the cowl inner surface, is positive. The net pitching moment is nose down since the nose-down moment acting on the ramp is dominant. The lift is about one and a half times larger than the thrust. All forces and moment with external flow are 7–36% smaller than those without external flow, as expected from the centerline pressure measurements and oil flow results. These large differences emphasize the importance of considering the external flow effects, especially the effect on the ramp side region pressure, in nozzle performance predictions.

Figure 20 compares the nozzle performance for SF-2 and SF-3. Obviously, the side fence length has a significant effect on the lift and the pitching moment, yet its effect on the thrust is relatively small, because thrust is primarily gained on the cowl inner surface on which the pressure is barely affected by the external flow. The thrust for SF-3 is 3.4% larger than that with SF-2, because the expansion of the exhaust in the ramp side regions is suppressed by a longer side fence. Under real flight conditions, where a lower specific heat ratio is present for the engine exhaust flow, the contribution of the ramp to the thrust would probably be larger; therefore, the effect of side fence length on the thrust becomes more important. The estimated values of thrust, lift, and pitching moment by the two-dimensional MOC agree well with the experimental values for SF-3. Therefore, this method is considered effective for preliminary designs of a scramjet nozzle having fairly two-dimensional flow.

Conclusions

An experimental investigation of scramjet asymmetric nozzle flowfields, including a hypersonic external flow in perfect gas conditions, was conducted in a hypersonic wind tunnel with a Mach number of 7.1. An external plume shock, a shear layer, and an intercepting shock generated near the cowl trailing edge were observed in schlieren photographs. Crossflow separations of the exhaust flow on the ramp, and a separated region on the cowl upper surface near the trailing edge were detected in surface oil flow tests. Surface and pitot pressure measurements showed that in underexpansion condition the external flow affected the surface pressure (i.e., nozzle performance) only from the ramp sides because the intercepting shock did not impinge on the ramp surface. In contrast, in overexpansion conditions, the external flow directly affected the surface pressure through a shock impingement upon the ramp. It was also found that the external flow effectively restrained the outward expansion of the exhaust flow, and delayed the boundary-layer separation on the ramp side regions and near the ramp aft end. An integration of the surface pressure measurements revealed that the external flow had significant effects on nozzle lift, thrust, and pitching moment. With a long-length side fence, the spanwise expansion of the exhaust flow was suppressed, thus, a slight thrust increase was obtained. The nozzle performance prediction by the two-dimensional method of characteristics with boundary-layer correction agreed well with the experimental results, thereby showing the effectiveness of the method in the cases the nozzle flowfield was fairly two-dimensional.

Acknowledgments

The wind-tunnel tests were performed with assistance from personnel at the National Aerospace Laboratory Hypersonic Wind Tunnel Facilities and Instrumentations Laboratories, especially Kiyomichi Ishida. This support is gratefully appreciated.

References

[1]Schetz, J. A., Billig, F. S., and Favin, S., "Numerical Solutions of Scramjet Nozzle Flows," *Journal of Propulsion and Power*, Vol. 3, No. 5, 1987, pp. 440–447.

[2]Harloff, G. J., Lai, H. T., and Nelson, E. S., "Two-Dimensional

Viscous Flow Computations of Hypersonic Scramjet Nozzle Flowfields at Design and Off-Design Conditions," AIAA Paper 88-3280, July 1988.

[3]Baysal, O., Engelund, W. C., Eleshaky, M. E., and Pittman, J. L., "Adaptive Computations of Multispecies Mixing Between Scramjet Nozzle Flows and Hypersonic Freestream," AIAA Paper 89-0009, Jan. 1989.

[4]Ruffin, S. M., Venkatapathy, E., Keener, E. R., and Nagaraj, N., "Computational Design Aspects of a NASP Nozzle/Afterbody Experiment," AIAA Paper 89-0446, Jan. 1989.

[5]Hopkins, H. B., Konopka, W., and Leng, J., "Validation of Scramjet Exhaust Simulation Technique at Mach 6," NASA CR-3003, Mar. 1979.

[6]Mitani, T., "Performance of Scramjet Nozzles," AIAA Paper 92-3290, July 1992.

[7]Pittman, J. L., "A Mach 6 External Nozzle Experiment with Argon-Freon Exhaust Simulation," Society of Automotive Engineers TP-892315, Sept. 1989.

[8]Ruffin, S. M., Venkatapathy, E., Lee, S. H., Keener, E. R., and Spaid, F. W., "Single Expansion Ramp Nozzle Simulations," AIAA Paper 92-0387, Jan. 1992.

[9]Shirouzu, M., Matsushima, K., and Nomura, S., "A Parametric Sensitivity Study on the Ascent of a SSTO," *Proceedings of the 16th International Symposium on Space Technology and Science*, AGNE Publishing Inc., Tokyo, May 1988, pp. 1527–1534.

[10]Hiraki, H., Hashimoto, N., Hashizume, H., Mohri, H., Yoshizawa, A., Nagasu, H., Ushida, K., and Hosoi, S., "Design and Construction of the 50cm Hypersonic Wind Tunnel at National Aerospace Laboratory," National Aerospace Lab. TR-116, Sept. 1966 (in Japanese).

[11]Tucker, M., "Approximate Calculation of Turbulent Boundary-Layer Development in Compressible Flow," NACA TN-2337, April 1951.

[12]Adamson, T. C., and Nicholls, J. A., "On the Structure of Jets from Highly Underexpanded Nozzles into Still Air," *Journal of the Aerospace Sciences*, Vol. 26, Jan. 1959, pp. 16–24.

[13]Papamoschou, D., and Roshko, A., "The Compressible Turbulent Shear Layer: An Experimental Study," *Journal of Fluid Mechanics*, Vol. 197, Dec. 1988, pp. 453–477.

[14]Chinzei, N., Masuya, G., Komuro, A., Murakami, A., and Kudou, K., "Spreading of Two-Stream Supersonic Turbulent Mixing Layers," *Physics of Fluids*, Vol. 29, No. 5, 1986.